Combined Power and Refrigeration From a Hot Stream

Juan C. ORDÓÑEZ, Jose V. C. VARGAS and Adrian BEJAN
Department of Mechanical Engineering and Materials Science,
Box 90300, Duke University, Durham, NC 27708-0300 - USA
E-Mail: abejan@duke.edu

Abstract

This paper outlines the thermodynamic optimization of a combined power and refrigeration system subject to constraints. In the first part, the system operates in the refrigeration mode and is driven by a hot stream of single-phase fluid that is subsequently discharged into the ambient. The irreversibility is due to three heat exchangers and the discharging of the used stream. It is shown that the thermodynamic optimum is pinpointed by an optimal ratio between the mass flow rates of the hot stream and the stream that is heated by the hot stream, and by an optimal distribution of the heat exchanger inventory among the three heat exchangers of the installation. The second part of the paper considers the more general situation where the system delivers power and refrigeration, and where the irreversibility is due additionally to the internal parts of the system. It is shown that the thermodynamic optimum is reached by distributing optimally the heat exchanger inventory among the three heat exchangers, and that this optimum is sensitive to the total inventory and the degree of irreversibility of the internal parts. It is also shown that the optimum is robust with respect to changes in several physical parameters.

Key words: entropy generation minimization, EGM, thermodynamic optimization.

1. Introduction

The methods of exergy analysis (EA), entropy generation minimization (EGM) and thermoeconomics (TE) are the most established forms of the changes that have taken place in modern engineering thermodynamics (Bejan, 1982, 1988, 1996; Feidt, 1987; Krane, 1994, 1995; Moran, 1982; Moran and Sciubba, 1994; Richter, 1993; Stecco and Moran, 1993). The emphasis is now on identifying the mechanisms and system components that are responsible for thermodynamic losses (EA), minimizing the losses subject to the global constraints of the system (EGM), and minimizing the total costs associated with building and operating the energy system (TE). Thermodynamic optimization may be used by itself (without cost minimization) in the preliminary stages of design (Bejan et al., 1996), in order to identify trends and the existence of optimization opportunities. The optima and structural characteristics identified based on thermodynamic optimization can be made more realistic through subsequent refinements based on global cost minimization.

The integrative design philosophy that is emerging from such applications can be summarized as follows: an entire system can be conceived from the beginning as a system designed to perform certain global objectives optimally, not as an ensemble of already existing parts.

This approach can be illustrated with reference to the objectives of power generation and refrigeration. Power or refrigeration systems are assemblies of streams and hardware (components). The size of the hardware is always constrained (e.g., weight, volume). Each stream carries exergy (useful work content), which is the life blood of the power system, i.e., another form of the fuel burnt to drive the system. Exergy is destroyed (or entropy is generated) whenever streams interact with each other and with components. The design objectives are: (i) to optimize streams and components so that they generate minimum entropy subject to constraints, and (ii) to make sure that the optimized entities "match", or can be "fitted" together (wrapped around each other) into a new integrative design of the larger system.

We used this approach in a first paper (Bejan and Errera, 1998) in which we proposed the most basic problem of this type in power generation: how to extract most exergy from a stream of hot gas, when the heat transfer surface available for cooling the stream is fixed. We showed that objective (i) is met when the stream and surface temperatures vary exponentially with the distance traveled by the stream, such that the stream-to-surface temperature difference is proportional to the local stream temperature. Objective (ii) is met by placing another single-phase stream on the cold side of the heat transfer surface, and by orienting this stream in counterflow with the hot stream. The capacity rate of the cold stream must be set at an optimal level, which is determined based on EGM.
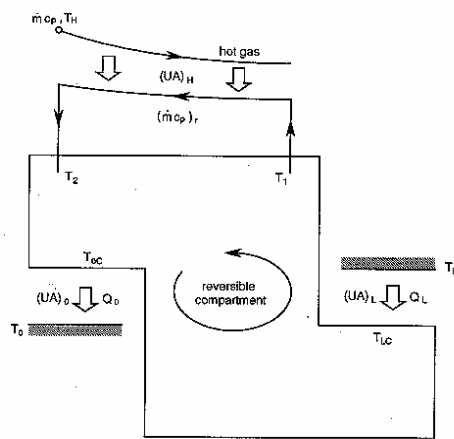

Figure 1. Model of combined power and refrigeration system driven by a hot stream through a counterflow heat exchanger.

In this paper we consider the thermodynamic optimization of a combined power and refrigeration system that is driven by a hot stream (*Figure 1*). We do this in two different settings. In the first, we focus on the optimal coupling that must be made between the given hot stream and the stream of fluid that circulates inside the combined system (section 2). To accomplish this in the clearest terms we isolate the "coupling" aspect of the optimization problem by adopting two limiting simplifications: the net power of the combined system to zero (i.e., all the generated power is used for refrigeration), and the irreversibility of the system is due entirely to the heat transfer processes that occur in the three heat exchangers of the system.

In the second part (section 3), we investigate systematically the two effects that were neglected in the first part. Specifically, we consider the more general class of combined systems that generate net power in addition to performing the combined

power-refrigeration internal function. The combined system generates entropy in all its parts, not just in its three heat exchangers.

2. Optimal Coupling With the Hot Stream

Consider the arrangement shown in *Figure 1*. A single-phase stream of flow rate $\dot{m}$ and initial temperature T_H heats an installation that draws heat at the rate $\dot{Q}_L$ from the temperature T_L, while rejecting $\dot{Q}_0$ to the ambient temperature T_0. The sizes of the three heat exchangers are characterized by the overall thermal conductances C_H, C_L and C_0. Each of these thermal conductances is shorthand for a product of type UA, where A is the actual contact area through which the respective heat transfer rate passes, and U is the overall heat transfer coefficient based on A.

In our first study of the thermodynamic optimization of the use of a hot stream (Bejan and Errera, 1998) we showed that the temperature gap between the hot-stream and the entity that receives the heat input must vary such that at every point on the heat transfer surface it is proportional to the local absolute temperature of the hot stream. We also showed that this temperature gap distribution can be materialized in a counterflow heat exchanger where the cold stream also carries a single-phase fluid. This configuration has been chosen for the hot end of the installation of *Figure 1*, where $(\dot{m}\,c_p)_r$ is the capacity rate of the stream that receives the heat input. In summary, the use of the counterflow arrangement in *Figure 1* is already an optimal feature. We adopt this feature from Bejan and Errera (1998) in order to abbreviate the remaining optimization work, which is the object of this section.

The receiving stream $(\dot{m}\,c_p)_r$ drives the main body of the installation, which is modeled as irreversibility free in the space delineated by the solid line in *Figure 1*. Applied to this space, the first law and the second law require
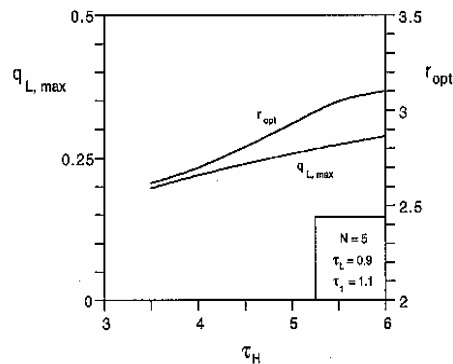

Figure 2. The maximized refrigeration rate and the optimal capacity rate ratio of the counterflow in the system of Figure 1.

$$\left(\dot{m}c_p\right)_r \left(T_2-T_1\right)+\dot{Q}_L-\dot{Q}_0=0 \qquad (1)$$

$$\left(\dot{m}c_p\right)_r \ln\frac{T_2}{T_1}+\frac{\dot{Q}_L}{T_{LC}}-\frac{\dot{Q}_0}{T_{0C}}=0 \qquad (2)$$

where T_{LC} and T_{0C} are the temperatures of the boundary portions crossed by $\dot{Q}_L$ and $\dot{Q}_0$. According to the simplest heat transfer model, these two heat transfer rates are assumed proportional to their respective conductances and temperature differences,

$$\dot{Q}_0=C_0\left(T_{0C}-T_0\right) \qquad (3)$$

$$\dot{Q}_L=C_L\left(T_L-T_{LC}\right) \qquad (4)$$

The counterflow heat exchanger is described by the effectiveness-N_{tu} relations,

$$\varepsilon=\frac{1-\exp\left[-N_H(1-r)\right]}{1-r\cdot\exp\left[-N_H(1-r)\right]}; \qquad N_H=\frac{C_H}{\dot{m}c_p} \quad (r<1) \quad (5a)$$

$$\varepsilon=\frac{1-\exp\left[-N_H\left(1-r^{-1}\right)\right]}{1-r^{-1}\exp\left[-N_H\left(1-r^{-1}\right)\right]} \qquad (r>1) \qquad (5b)$$

$$T_2-T_1=\varepsilon r\left(T_H-T_1\right); \quad r=\dot{m}c_p/\left(\dot{m}c_p\right)_r \quad (r<1) \qquad (6a)$$

$$T_2-T_1=\varepsilon\left(T_H-T_1\right) \qquad (r>1) \qquad (6b)$$

where r and N_H are the capacity rate ratio, and the number of heat transfer units of the hot-end heat exchanger. The corresponding numbers for the other two heat exchangers are defined similarly, $N_0 = C_0/(\dot{m}c_p)$ and $N_L = C_L/(\dot{m}c_p)$. The finite
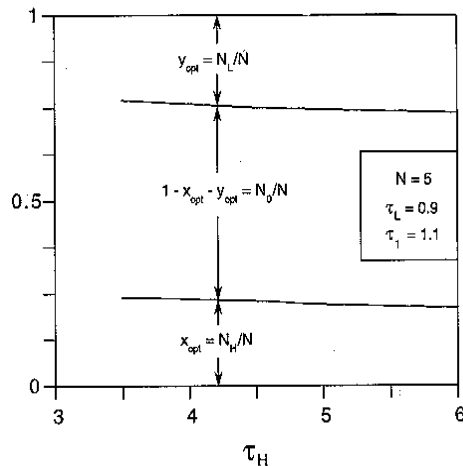

Figure 3. The effect of the hot-stream inlet temperature on the optimal allocation of heat exchanger inventory in the system of Figure 1.

heat exchanger inventory is described in the simplest terms (Bejan, 1988, 1996) by the conductance constraint $C_H + C_0 + C_L = C$ or, after writing $N = C/(\dot{m}c_p)$ for the total number of heat transfer units, by the total N constraint.

$$N_H+N_0+N_L = N \qquad (7)$$

Equations (1) - (4) and (6) can be non-dimensionalized by introducing the notation

$$\tau=\frac{T}{T_0} \qquad q_0=\frac{\dot{Q}_0}{\dot{m}c_p T_0} \qquad q_L=\frac{\dot{Q}_L}{\dot{m}c_p T_0} \qquad (8)$$

They become, in order,

$$\tau_2-\tau_1+r\left(q_L-q_0\right)=0 \qquad (9)$$

$$\ln\frac{\tau_2}{\tau_1}+r\left(\frac{q_L}{\tau_{LC}}-\frac{q_0}{\tau_{0C}}\right)=0 \qquad (10)$$

$$q_0=N_0\left(\tau_{0C}-1\right) \qquad (11)$$

$$q_L=N_L\left(\tau_L-\tau_{LC}\right) \qquad (12)$$

$$\tau_2-\tau_1=\varepsilon r\left(\tau_H-\tau_1\right) \qquad (13)$$

In summary, the analytical model consists of six equations, namely Eqs. (5) and (9) - (13), which must be solved for six unknowns: q_0, q_L, ε, τ_2, τ_{0C} and τ_{LC}. The seven specified numerical parameters are τ_H, τ_L, τ_1, r, N_H, N_0 and N_L. In view of the N constraint (7), the numbers N_H, N_0 and N_L may be replaced by (i.e., deduced from) the total number N and the conductance allocation fractions

$$x=\frac{N_H}{N} \qquad y=\frac{N_L}{N} \qquad 1-x-y=\frac{N_0}{N} \qquad (14)$$

The objective is to maximize q_L, which represents the refrigeration effect that is ultimately due to the spent stream of hot fluid. The numerical work consisted of using Eqs. (5) and (9) - (13) to develop q_L as a function of the seven parameters. The system of six equations was first reduced to four equations, by noting that for a given set of parameters ε and τ_2 can be calculated directly from Eqs. (5) and (13). The remaining four equations, namely Eqs. (9)-(12) were reduced via analytical substitution to a single equation. The latter was solved numerically for q_L using a code based on the Newton-Raphson and bisection methods, coupled with a search for appropriate initial guesses. Convergence was achieved in all the solutions by imposing the tolerance level $|F(q_L)|^2 \le 10^{-8}$. Finally, the remaining unknowns (q_0, τ_{0C}, τ_{LC}) were calculated as soon as q_L was determined.
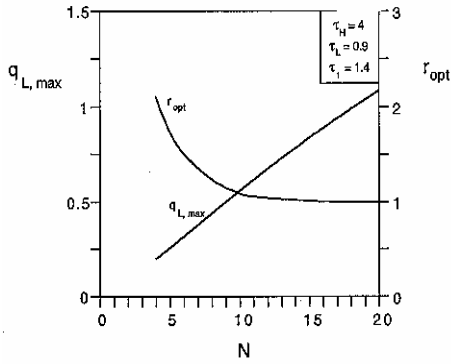
Figure 4. The effect of the total heat exchanger inventory on the maximized refrigeration rate and the optimal capacity rate ratio.
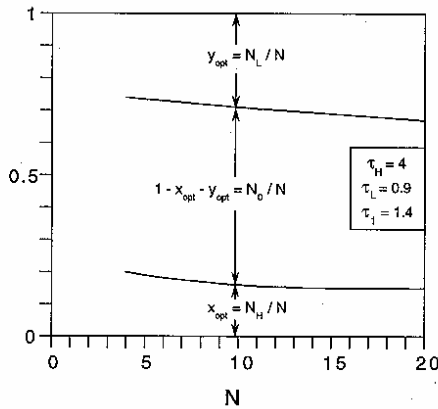

Figure 5. The effect of the total heat exchanger inventory on the optimal allocation of heat transfer area in the system of Figure 1.

In the first phase of the numerical work we assigned representative order-of-magnitude values to the "external" parameters τ_H, τ_L, τ_1 and N, and maximized q_L with respect to the "internal" parameters r, x and y. The r ratio controls the coupling between the hot stream and the rest of the installation. The ratios (x, y) dictate how the heat exchanger inventory is distributed through the system.

Figures 2 and 3 show the first results of this 3-way optimization. The procedure was repeated for several hot-stream temperatures covering the range $3.5 \leq \tau_H \leq 6$. The maximized refrigeration rate and the optimal capacity rate ratio (the match parameter r_{opt}) increase monotonically as τ_H increases (*Fig. 2*). The relative allocation of heat exchanger inventory (x_{opt}, y_{opt}, $1 - x_{opt} - y_{opt}$) is almost insensitive to changes in τ_H, as shown in *Fig. 3*. The values of the external parameters held fixed in *Figs. 2 and 3* (namely, N, τ_L and τ_1) are such that the physical parameters of the system of *Fig. 1* obey the following relations: $T_{0C} > T_0$, $\dot{Q}_0 > \dot{Q}_L$, $0 < T_{LC} < T_L$, and $T_{0C} < T_{HC}$, where
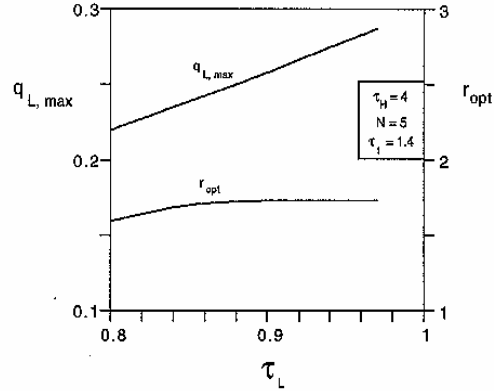
Figure 6. The effect of the refrigeration temperature on the maximized refrigeration rate and the optimal capacity rate ratio.

T_{HC} is the effective temperature level of the $(\dot{m}c_p)_r$ stream, $T_{HC} = (T_2 - T_1)/\ln(T_2/T_1)$.

The effect of the total heat exchanger inventory is documented in *Figs. 4 and 5* in the range $4 \leq N \leq 20$. The maximized refrigeration rate increases almost linearly with N. The optimized capacity rate ratio decreases and approaches asymptotically $r_{opt} = 1$ as N becomes greater than 10. The optimal distribution of heat exchanger size is somewhat more sensitive to N: the fraction allocated to the refrigeration end (y_{opt}) decreases monotonically as N increases, while x_{opt} becomes constant when N exceeds 10.
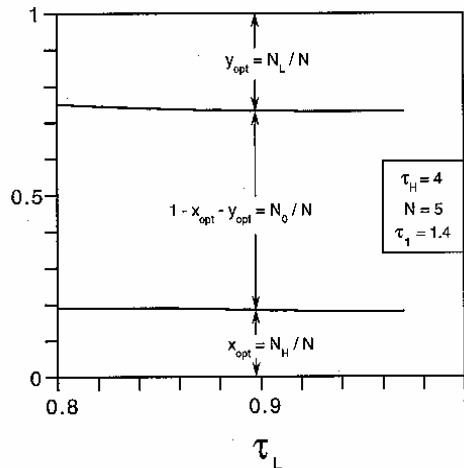

Figure 7. The effect of the refrigeration temperature on the optimal allocation of heat transfer area in the system of Figure 1.

Figures 6 and 7 document the effect of the refrigeration level τ_L. As expected, the maximized refrigeration rate increases as τ_L approaches 1, i.e., as T_L approaches the ambient T_0. The matching ratio r_{opt} increases to a plateau value of order 1.7

as τ_L rises above 0.9. The relative allocation of heat exchanger inventory is practically insensitive to τ_L. In other words, the physical characteristics of the thermodynamically optimal design are robust with respect to changes in the refrigeration temperature level.
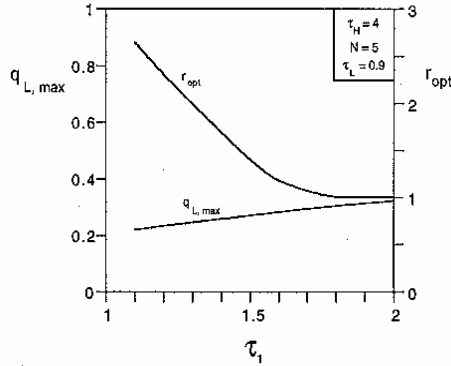

Figure 8. The effect of the matching stream inlet temperature on the maximized refrigeration rate and the optimal capacity rate ratio
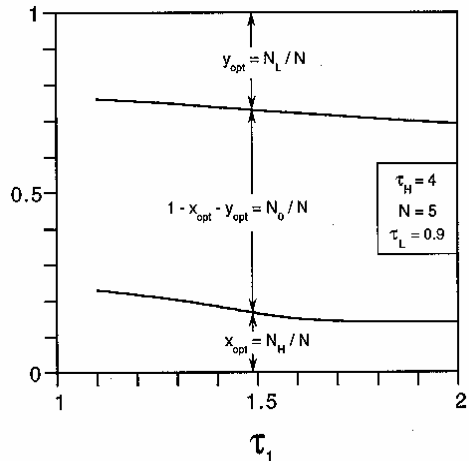

Figure 9. The effect of the matching stream inlet temperature on the optimal allocation of heat transfer area in the system of Figure 1.

The effect of the matching stream inlet temperature τ_1 is presented in *Figures 8* and *9*. As τ_1 becomes larger the optimal capacity rate ratio approaches 1, which means that the optimal counterflow is the balanced arrangement. The area allocation fractions x_{opt} and y_{opt} decrease weakly as τ_1 increases, and this means that the area allocated for heat transfer with the ambient $(1 - x_{opt} - y_{opt})$ remains practically unchanged. In summary, *Figs. 3, 5, 7 and 9* show that the optimal distribution of the fixed heat exchanger inventory is relatively insensitive to changes in τ_H, N, τ_L and τ_1.

3. Other Irreversibilities, and the Effect of Net Power

In the model of *Figure 10* we propose to examine how the thermodynamic optimum is influenced by two important features that were not included in *Figure 1*. First, not all the generated power is used for generating the refrigeration effect $\dot{Q}_L$: the remaining fraction is delivered as net power $\dot{W}$ to an external user. The operation of the combined system may span the entire spectrum from pure refrigeration to pure power production, and its position on this scale is marked by the ratio $R = \dot{Q}_L / \dot{W}$.

The second new feature is the irreversibility of the system, which now characterizes the interior of the power and refrigeration installation, not just the three heat exchangers. We account for this feature by means of the exergetic efficiency η_{II} of the system defined by the solid line in *Figure 10*. The specified parameter η_{II} is less than 1, and is defined as the ratio of the net exergy flow rate out of the system divided by the net flow of exergy into the system.
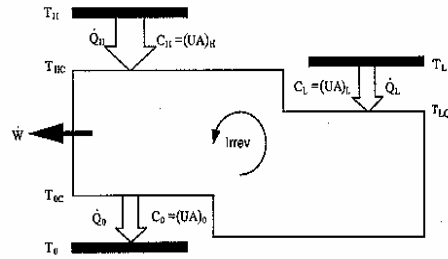

Figure 10. Model of combined power and refrigeration system with internal irreversibility.

To accommodate these new features while keeping the analysis and graphics simple enough to reveal the effect of these particular features, in *Figure 10* we opted for a simpler hot-end heat exchanger model. The heat input rate $\dot{Q}_H$ is a fixed (given) parameter, and replaces the flow rate of hot fluid $(\dot{m})$ of *Figure 1*. The receiving stream $(\dot{m}_r)$ is replaced by the region of lower temperature T_{HC} on the solid-line boundary. Equations (5, 6) are now replaced by

$$\dot{Q}_H = C_H (T_H - T_{HC}) \qquad (15)$$

and instead of the first law (1) and the second law (2) we have

$$\dot{Q}_H + \dot{Q}_L - \dot{Q}_0 - \dot{W} = 0 \qquad (16)$$

$$\dot{S}_{gen} = \frac{\dot{Q}_0}{T_{0C}} - \frac{\dot{Q}_L}{T_{LC}} - \frac{\dot{Q}_H}{T_{HC}} \geq 0 \qquad (17)$$

Equations (3) and (4) continue to apply. For the nondimensionalization of these equations we continue to use $\tau = T/T_0$, however, the remaining variables and parameters have to be redefined,

$$\hat{q}_0 = \frac{\dot{Q}_0}{\dot{Q}_H} \qquad \hat{q}_L = \frac{\dot{Q}_L}{\dot{Q}_H} \qquad w = \frac{\dot{W}}{\dot{Q}_H} \qquad (18)$$

$$\left(\hat{N}_H, \hat{N}_0, \hat{N}_L, \hat{N}\right) = \frac{T_0}{\dot{Q}_H} \left(C_H, C_0, C_L, C\right) \qquad (19)$$

$$x = \hat{N}_H / \hat{N} \quad y = \hat{N}_L / \hat{N} \quad 1-x-y = \hat{N}_0 / \hat{N} \quad (20)$$

In summary, the dimensionless equations that govern the functioning of the model of *Figure 10* are

$$1 + \hat{q}_L - \hat{q}_0 - w = 0 \qquad (21)$$

$$\eta_{II} = \frac{\hat{q}_0 \left(1 - \tau_{0C}^{-1}\right) + w}{1 - \tau_{HC}^{-1} + \hat{q}_L \left(1 - \tau_{LC}^{-1}\right)} \leq 1 \qquad (22)$$

$$1 = x \, \hat{N} \left(\tau_H - \tau_{HC}\right) \qquad (23)$$

$$\hat{q}_0 = (1-x-y) \, \hat{N} \left(\tau_{0C} - 1\right) \qquad (24)$$

$$\hat{q}_L = y \, \hat{N} \left(\tau_L - \tau_{LC}\right) \qquad (25)$$
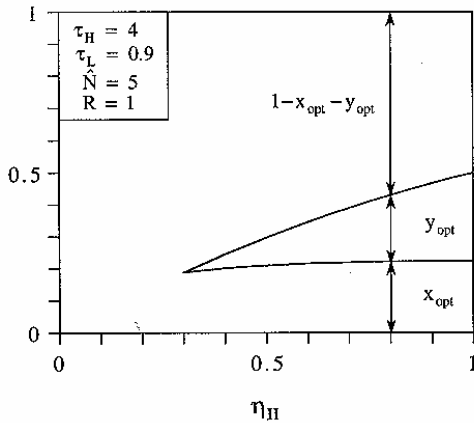
$$\hat{q}_L = R \, w \qquad (26)$$

Figure 11. The optimal distribution of heat exchanger inventory, as a function of the second-law efficiency of the power and refrigeration system.

where the second-law efficiency statement (22) accounts for the second law (17). The system of six equations (21) - (26) was solved numerically for the six unknowns: w, $\hat{q}_0$, $\hat{q}_L$, τ_{HC}, τ_{0C}, and τ_{LC}. These were developed numerically as functions of the remaining parameters: x, y, τ_H, τ_L, $\hat{N}$, η_{II} and R.

In the first stage of this numerical work we maximized the specific work output with respect to

the spatial distribution of heat exchanger inventory, x and y. Next, we investigated the impact of the internal irreversibility (η_{II}) and the mode of operation (R) on the thermodynamic optimum. The external temperature ratios (τ_H, τ_L) and the total heat exchanger inventory ($\hat{N}$) were assumed specified.

Figure 11 shows how the distribution of heat exchanger equipment responds to changes in the internal second-law efficiency, when the operating mode ratio is set at $R = 1$. The sizes of the three heat exchangers are plotted in relative terms, so that the three sizes always add up to 1. The figure shows that the size of the hot-end heat exchanger (x_{opt}) is relatively insensitive to changes in η_{II}. The other two heat exchangers respond together: the refrigeration-load heat exchanger decreases in size as η_{II} decreases, and vanishes entirely at approximately $\eta_{II} = 0.3$. The power output and refrigeration effect also vanish at this point, as shown by the corresponding dashed line in *Fig. 12*. This behavior has its source in the irreversibility of the combined system. When η_{II} is too low, all the exergy that is available based on $\dot{Q}_H$ [namely $\dot{Q}_H (1 - T_0/T_H)$], is destroyed through the irreversibility of the power and refrigeration installation. *Figure 12* also shows the corresponding behavior of the temperature gaps of the three heat exchangers.
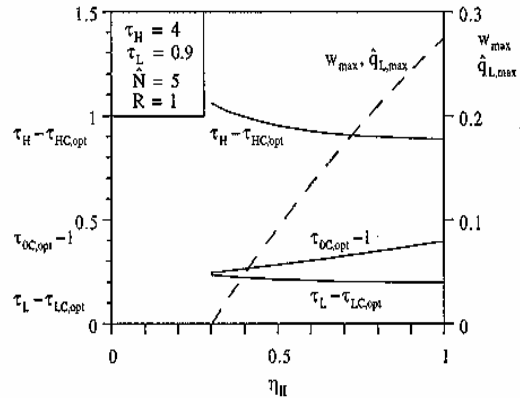

Figure 12. The maximized power and refrigeration, and the three temperature gaps that correspond to the system optimized in Figure 11.

Figures 13 and *14* show the effect of the operating mode ratio R, when η_{II} is fixed. As the installation works more as a refrigerator, the maximized power output decreases, and the size fractions x_{opt} and y_{opt} converge on the same R-independent value of about 20 percent. In other words, where R increases the hot-end heat exchanger shrinks at the expense of the refrigeration-load heat exchanger, and this trend becomes less noticeable when R exceeds the order of 1. The

temperature gaps spanned by the three heat exchangers (*Fig. 14*) increase as R increases, and become insensitive to R as R exceeds the order of 1.

The refrigeration temperature τ_L influences only weakly the optimal allocation of the heat exchanger inventory, *Figure 15*. The maximized power and refrigeration rate increase as τ_L increases. These trends agree qualitatively with the trends revealed by the optimization of the first model (*Fig. 1*), which were documented in *Figures 6 and 7*.

The effect of the total heat exchanger inventory is also similar to what we saw based on the first model. *Figure 16* shows that the maximized refrigeration rate and power output increase as $\hat{N}$ increases. The area fractions x_{opt} and y_{opt} exhibit competing changes; at the same time, the area reserved for heat transfer with the ambient $(1 - x_{opt} - y_{opt})$ remains practically constant, which is a conclusion similar to what we found based on the middle section of *Figure 5*.
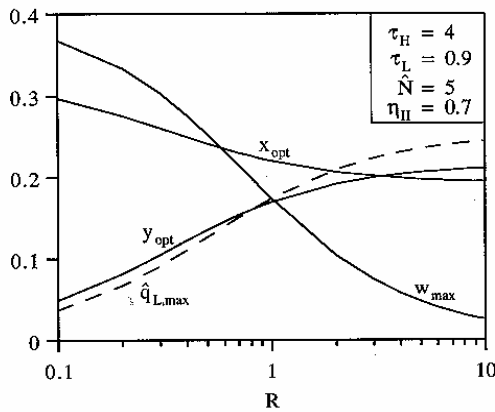

Figure 13. The maximized power and refrigeration, and the optimal distribution of heat exchanger inventory as functions of the operating mode ratio R.

4.   The Minimization of Entropy Generation

It remains to show that the simultaneous maximization of power output and refrigeration, on which the preceding results are based, is completely equivalent to the minimization of entropy generation in the entire system. The entropy generation rate in the entire system—the heat exchangers plus the inner space in *Figure 10*—is given by

$$\dot{S}_{gen}^{total} = \frac{\dot{Q}_0}{T_0} - \frac{\dot{Q}_H}{T_H} - \frac{\dot{Q}_L}{T_L} \geq 0 \qquad (27)$$

Next, we eliminate $\dot{Q}_0$ between Eq. (27) and the

first law (16), replace $\dot{Q}_L$ by $R\,\dot{W}$, and obtain

$$\dot{W} = \frac{\dot{Q}_H\left(1 - T_0/T_H\right) - T_0\,\dot{S}_{gen}}{1 - R\left(1 - T_0/T_L\right)} \qquad (28)$$

This expression shows that in these circumstances, i.e., when $\dot{Q}_H$ and R are specified, the maximization of $\dot{W}$ (or $\dot{Q}_L$) is completely equivalent to the minimization of the entropy generation rate.

5.   Conclusions

In this paper we conducted the thermodynamic optimization of a combined power and refrigeration system that is driven by a hot stream of single-phase fluid, while in contact with the ambient. The interface between the system and the hot stream was provided by a counterflow heat exchanger, which is a known thermodynamic optimization feature (Bejan and Errera, 1998). The total number of heat transfer units of the three heat exchangers (hot stream, refrigeration load, ambient) was constrained.
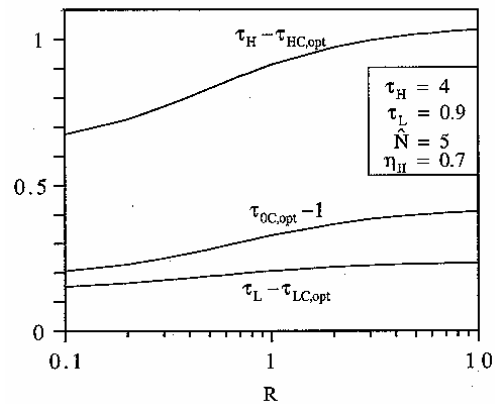

Figure 14. The three temperature gaps that correspond to the thermodynamic optimum of Figure 13.

In the first part of the paper we considered the simpler setting where the system works in the pure refrigeration mode. The irreversibility of the system-ambient arrangement was due to the three heat exchangers and the discharging of the used hot stream into the ambient. We located the thermodynamic optimum by maximizing the refrigeration load subject to the heat exchanger inventory constraint and the fixed flow rate and inlet temperature of the hot stream. We showed that the thermodynamic optimum is characterized by (i) a special ratio between the flow rate of the hot stream and the flow rate of the heat-receiving stream employed by the system (*Fig. 2*), and (ii) an

optimal distribution of the heat exchanger inventory between the three heat exchangers (*Fig. 3*). The sensitivity of the optimal operating conditions relative to changes in the physical parameters of the system was documented systematically.

In the second part of the paper we investigated the performance of a more general model with net power generation (in addition to refrigeration), and entropy generation in the internal parts other than the heat exchangers. Constrained were the total heat exchanger inventory and the heat input rate. We found that the thermodynamic optimum is attained through an optimal distribution of the heat exchanger inventory between the three heat exchangers (*Fig. 11*). This feature is sensitive to changes in the mode of operation (refrigeration vs. power; R), the total heat exchanger inventory, and the degree of irreversibility of the internal parts.

Figure 16. The maximized power and refrigeration, and the optimal distribution of heat exchanger inventory as functions of the total heat exchanger inventory.
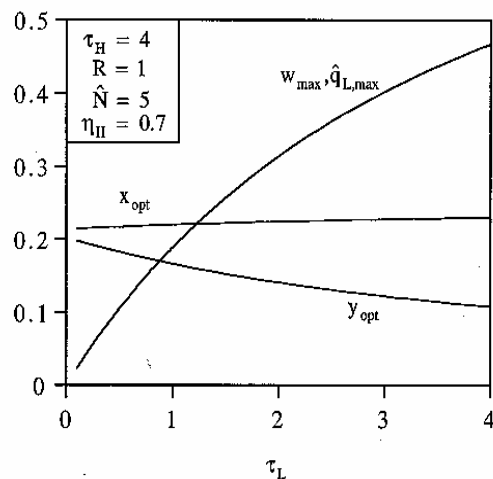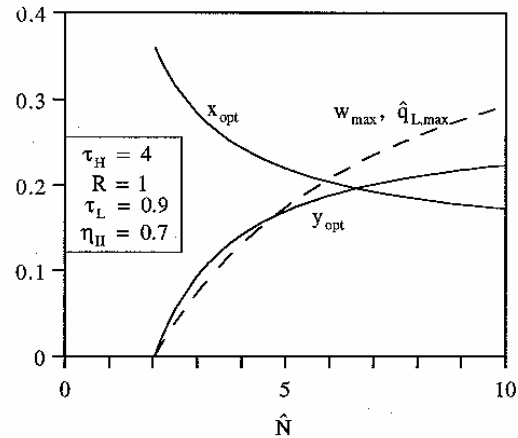
Figure 15. The maximized power and refrigeration, and the optimal distribution of heat exchanger inventory as functions of the refrigeration temperature level.

In summary, this study showed that opportunities for optimizing the operation of combined power and refrigeration systems can be identified based on the thermodynamic optimization of relatively simple realistic models that include economic considerations (Bejan et al., 1996). Once identified, these optimization opportunities deserved to be pursued in engineering practice, based on considerably more systems parameters exert a strong influence on the thermodynamic optimum. The robustness of the optimum relative to certain parameters (e.g., load temperature, *Fig. 7*) may be used to simplify future optimizations of similar combined systems.

Nomenclature

A	heat transfer area, m^2
c_p	specific heat at constant pressure, J/kg K
C	thermal conductance, W/K
$\dot{m}$	mass flow rate, kg/s
$N, \hat{N}$	numbers of heat transfer units, Eqs. (5) and (19)
q_0, q_L	dimensionless heat transfer rates, Eqs. (8)
$\hat{q}_0, \hat{q}_L$	dimensionless heat transfer rates, Eqs.(18)
r	ratio of capacity rates, Eq. (6)
R	relative refrigeration load, $\dot{Q}_L / \dot{W}$
$\dot{S}_{gen}$	entropy generation rate, W/K
T	temperature, K
U	overall heat transfer coefficient, W/m^2 K
$\dot{W}$	power, W
w	dimensionless power, Eq. (18)
x, y	conductance allocation ratios, Eqs. (14) and (20)

Greek Symbols

ε heat exchanger effectiveness

η_{II} second law efficiency, Eq. (22)

τ dimensionless temperature, Eq. (8)

Subscripts

C   reversible compartment
H   high temperature
L   low temperature
r   receiving stream
0   ambient temperature

References

Bejan, A., 1982, *Entropy Generation through Heat and Fluid Flow*, Wiley, New York.

Bejan, A., 1988, *Advanced Engineering Thermodynamics*, Wiley, New York.

Bejan, A., 1996, *Entropy Generation Minimization*, CRC Press, Boca Raton.

Bejan, A. and Errera, M. R., 1998, "Maximum power from a hot stream," *Int. J. Heat and Mass Transfer*, Vol.41, pp.2025-2036.

Bejan, A., Moran, M. and Tsatsaronis, G., 1996, *Thermal Design and Optimization*, Wiley, New York.

Feidt, M., 1987, *Thermodynamique et Optimisation ⌈nergetique des Systemes et Procedes,* Technique et Documentation, Lavoisier, Paris.

Krane, R. J., ed., 1994, *Thermodynamics and the Design, Analysis, and Improvement of Energy Systems 1994*, AES-Vol. 33, ASME, New York.

Krane, R. J., ed., 1995, *Thermodynamics and the Design, Analysis, and Improvement of Energy Systems 1995*, AES-Vol. 35, ASME, New York.

Moran, M. J., 1982, *Availability Analysis: A Guide to Efficient Energy Use*, Prentice-Hall, Englewood Cliffs, NJ.

Moran, M. J. and Sciubba, E., 1994, "Exergetic analysis: principles and practice," *Journal of Engineering Gas Turbines and Power*, Vol.116, pp. 285-290.

Richter, H. J., ed., 1993, *Thermodynamics and the Design, Analysis and Improvement of Energy Systems 1993*, HTD-Vol. 266, ASME, New York.

Stecco, S. S. and Moran, M. J., 1992, *Energy for the Transition Age*, Nova Science, New York.